Electronic structure of hexagonal Al_5Co_2

1997 J. Phys.: Condens. Matter 9 9585

(http://iopscience.iop.org/0953-8984/9/44/013)

J. Phys.: Condens. Matter **9** (1997) 9585–9596. Printed in the UK PII: S0953-8984(97)83515-1

Electronic structure of hexagonal Al_5Co_2

Esther Belin-Ferré†+, Guy Trambly de Laissardière‡, Pierre Pecheur§, Anne Sadoc‖ and Jean Marie Dubois¶

† LCPMR, URA CNRS 176 and GDR CINQ, 11 rue P et M Curie, F-75231 Paris Cédex 05, France

‡ LEPES–CNRS and GDR CINQ, 25 Avenue des Martyrs, BP 166X, F-38042 Grenoble, and LLB, Bâtiment 563, CEA—Saclay, F-91191 Gif-sur-Yvette Cédex, France

§ LMPSM, URA CRNS 155 and GDR CINQ, Ecole des Mines, Parc de Saurupt, F-54042 Nancy Cédex, France

‖ LURE, Bâtiment 209A, 91405 Orsay Cédex, and LPMS and GDR CINQ, Université de Cergy-Pontoise, Bâtiment des Sciences de la Matière, Neuville sur Oise, F-95031 Cergy-Pontoise Cédex, France

¶ LSG2M, URA CNRS 159 and GDR CINQ, Ecole des Mines, Parc de Saurupt, F-54042 Nancy Cédex, France

Received 18 April 1997, in final form 7 August 1997

Abstract. We have investigated the electronic structure of hexagonal Al_5Co_2 through theoretical as well as experimental means. Two different calculations have been carried out within the LMTO and tight-binding–LMTO methods. The experimental procedure involved soft-x-ray spectroscopy complemented by photoemission measurements. Co states have been found near the Fermi level, in interaction with Al states of hybridized p, s–d character. As a result, a pseudo-gap is generated at the Fermi level. Occupied Al states beyond 5 eV form the Fermi level are found to be almost pure s in character. The comparison between the experimental results and calculations indicates a rather good agreement with results from LMTO, consistent with the fact that this is a more elaborate band structure calculation. Agreement is only acceptable with results from the TB–LMTO calculations but these can be improved with a more careful treatment of the TB structure constants.

1. Introduction

Electronic properties of approximants and quasicrystals have been found to be very similar (Berger 1994, Quivy *et al* 1996). It appears thus interesting to investigate the electronic structure of approximants because insight may be gained into that of the related quasicrystals. Song and Ryba (1992) have shown that hexagonal Al_5Co_2 is an approximant of the quasicrystalline decagonal phase with the shortest periodic stacking sequence along the tenfold axis. This has given impetus to the study of the energy distribution of its electronic states. To this end, we have used theoretical as well as experimental means. Preliminary results have been reported elsewhere (Pécheur *et al* 1995). They have been supplemented by new experimental results as well as a new calculation. Indeed the previous calculations were performed within the tight-binding method (TB) and the linear muffin-tin orbital method in the atomic sphere approximation (LMTO–ASA) (Andersen 1975). In this paper, we also

+ Contact author: Esther Belin-Ferré, Laboratoire de Chimie Physique—Matière et Rayonnement, URA CNRS 176 and GDR CINQ, 11 rue Pierre et Marie Curie, 75231 Paris Cédex 05, France. Tel: +33 1 44 27 66 20. Fax: +33 1 44 27 62 26. E-mail address: belin@ccr.jussieu.fr

0953-8984/97/449585+12$19.50

Table 1. Co-ordinates of atoms in the unit cell (Wyckoff notations) and interatomic distances (Newkirk *et al* 1961).

Atomic site	Wyckoff notations	x	y	z
Al (1)	2(a)	0	0	0
Co (1)	2(d)	$\frac{1}{3}$	$\frac{2}{3}$	$\frac{3}{4}$
Al (2)	6(h)	0.4702	0.9404	$\frac{1}{4}$
Co (2)	6(h)	0.1268	0.2536	$\frac{1}{4}$
Al (3)	12(k)	0.1946	0.3892	0.9420

report on results of a calculation of total and partial densities of states using a combination of TB and LMTO. The results are compared with experiments.

LMTO–ASA is the most elaborate method and is expected to give the best results. As a matter of fact, it is well known to give good self-consistent electronic structure calculations for metallic crystals. It is particularly well adapted to compact alloys with a small charge transfer between the atoms. However, TB methods are still widely used as they can be easily applied to complex structure, such as higher-order approximants and to the treatment of defects, vacancies, impurities or surfaces. So it seemed interesting to perform such TB calculations as well, in order to allow an assessment of the accuracy which can be expected from TB in the case of a transition metal compound with several types of atom in the unit cell.

The experimental investigation combines both soft-x-ray emission spectroscopy (SXES) and photoelectron spectroscopy (XPS) techniques. This makes it possible to describe separately occupied and unoccupied states and to adjust the electronic distributions in the binding energy scale.

The paper is organized as follows: section 2 presents, compares and discusses the DOS calculations. Section 3 describes the experimental techniques and the procedures carried out for the measurements and reports the results. Discussion and comparison between experimental and theoretical data is the matter of section 4. A general conclusion is given in section 5.

2. Calculations of densities of states

The atomic structure of Al_5Co_2 is hexagonal, with space group $P6_3/mmc$ and lattice parameters $a = 0.76560$ nm and $c = 0.75932$ nm. Each unit cell contains 28 atoms; it displays three different Al sites and two different Co sites. Their co-ordinates are given in table 1 in the notation of Wyckoff (Newkirk *et al* 1961).

2.1. Theoretical methods

In the LMTO–ASA calculation, a scalar relativistic code (Andersen 1975) was used as well as the local density approximation formulation of Hedin and Lundqvist (1971) for the exchange and correlation potential. The basis functions include orbitals of angular moment up to $l = 2$ for Al and Co. The valence states were thus Al 3s, 3p and 3d and Co 4s, 4p and 3d. The atomic structure of this crystal being fairly compact, it was not necessary to include empty spheres during the calculation. Within the ASA framework, the radii of the atomic spheres were chosen so that the total volume of the spheres equals the volume of the unit cell. These radii, which were used to build the muffin-tin orbitals, are $R_{Al} = 0.152$ nm and $R_{Co} = 0.140$ nm. This leads to a good compromise between

the sphere overlaps (which are less than 35–40%) and the charge transfer between spheres (which is smaller than 0.15 electrons/atom). Moreover we checked that the DOS does not change significantly when the radii are changed by 10%. The k integration was performed by the tetrahedron method (Jepsen and Andersen 1971), and convergence was searched for on a grid of 84 k points in the reduced Brillouin zone, i.e. 1000 k points in the first Brillouin zone. We checked that these sets were large enough.

It is noteworthy that the LMTO method can be adapted to TB calculations (Andersen *et al* 1985). Therefore, we have also performed a calculation within this TB–LMTO combination which we denote in the following as TB–LMTO. In the present case, the TB Hamiltonian that is obtained may be more accurate than the empirical TB Hamiltonian used in our previous work (Pécheur *et al* 1995) while retaining the initial simplicity of the method. The calculation uses the tabulated LMTO TB structure constants and potential parameters to obtain the matrix elements of the TB Hamiltonian. It allows us to take into account the dependence of the diagonal elements on the environment and the overlap between orbitals (in a perturbative way). The potential parameters are also dependent on the mean atomic volume per atom in the compound. No self-consistency was performed; the radii of the spheres were chosen to obtain neutrality in Al and Co spheres. Interactions were taken into account up to a distance of 0.38 nm. The partial DOSs were then calculated in real space with the recursion method on a cluster of 104 atoms (Haydock 1980). One hundred levels of the continuous fraction were obtained in a cluster of more than 8000 atoms.

2.2. Results and discussion

In the following Al 3s, Al 3d, Al 3p and Co 3d apply to the occupied distributions whereas Al s, Al d, Al p and Co d refer to the distributions normally unoccupied.

The general appearance of the band structures obtained from the various calculations is fairly much the same as shown in figure 1(a) from LMTO and 1(b) from TB–LMTO. Indeed, in all calculations, the Fermi level (E_F) lies in a deep minimum of the DOSs, total or partial, thus showing the presence of a pseudogap at E_F (Trambly de Laissardière *et al* 1995). The DOSs are dominated by the Co 3d states which spread over an energy range of about 2.5 eV from E_F. The energy of their maxima differs only slightly from one calculation to the other: it is 2.0 ± 0.1 eV and 2.1 ± 0.1 eV from E_F respectively within the LMTO and TB–LMTO methods.

The Al 3p states are mostly concentrated within the energy range that covers about 5 eV from E_F, then their intensity decreases rapidly. Al 3d-like states are always present near E_F in the same energy range as the Co 3d states. Their shape is rather reminiscent of that of the Co 3d DOSs; however, the relative intensities of the various peaks change from Co to Al. Let us mention that in all cases this Al 3d-like contribution near E_F is more important than that found in pure fcc Al (Papaconstantopoulos 1986).

Whatever the calculation is, the Al 3s states with significant intensity are found beyond about 4 eV from E_F. Note however that TB–LMTO shows the presence of a weaker peak at about 2.5 eV from E_F which is not observed in LMTO. The Al s DOSs in the TB–LMTO calculations exhibit numerous contrasted spikes beyond 5 eV from E_F. These are artefacts that have no physical signification. They may be ascribed to the fact that the s orbitals are the most extended ones and the cluster size is not sufficient to obtain high-order moments with enough accuracy which would give better s band edges. This problem is much less important for p orbitals and not present for d orbitals.

From the coincidence between features of the partial Al DOSs, we point out that Al states of hybridized p–d character are present in the vicinity of E_F over about 4 eV, retaining

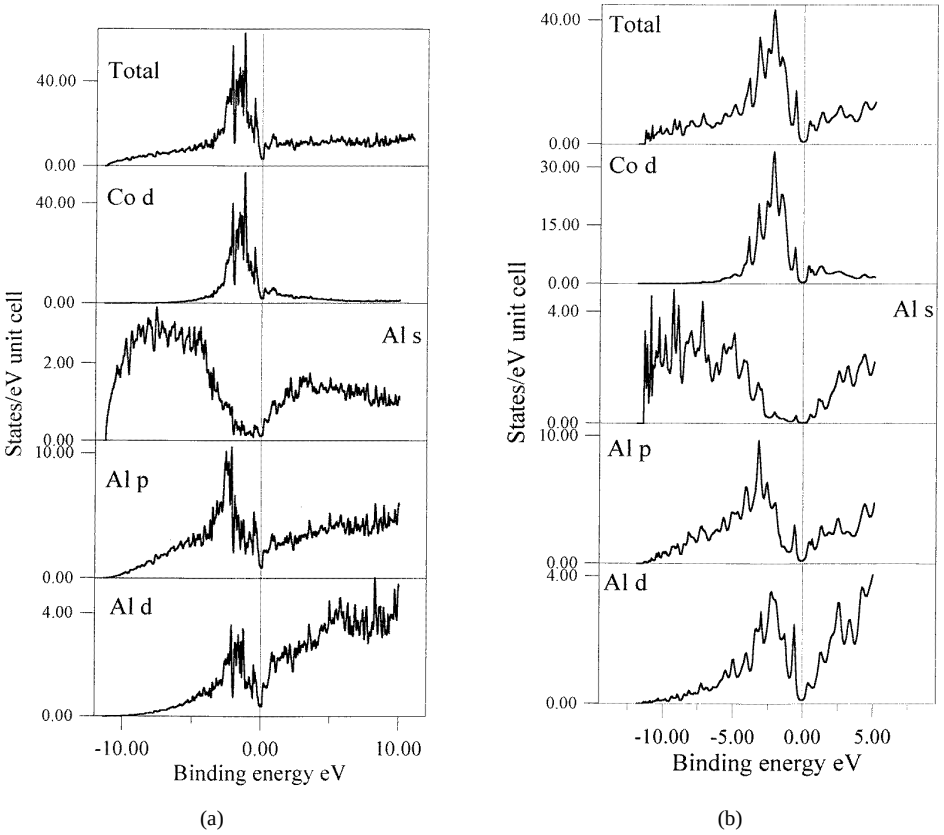

Figure 1. (a) Total and partial DOSs as calculated using the LMTO–ASA method: from top to bottom, total DOS, Co d, Al s, Al p and Al d partial DOSs. (b) Total and partial DOSs as calculated using the mixed TB-LMTO method: from top to bottom, total DOS, Co d, Al s, Al p and Al d partial DOSs.

however a more marked p-like character at about 2.6 eV from E_F. The interaction between Al and Co states differs according to their s, p or d character. The Al states with originally localized or somewhat localized character, namely p and d-like overlap in energy with localized Co 3d states. In this energy range, the Al s states are of very faint intensity. This indicates that the Al–Co interaction must be of Fano-like nature, i.e. interaction between localized and extended states. This kind of interaction has been discussed by Terakura (1977), who emphasized that (i) the d-like states are shifted from the energy position they had without interaction, (ii) the extended states split into two distinct bonding and non-bonding parts located on each side of the energy position of the maximum of the d states and (iii) these extended states exhibit a relative minimum intensity, the so-called hybridization gap, that is at the energy of the maximum of the d state distribution.

In Al_5Co_2, because of this type of interaction, intense Al 3p states are shifted by about 1 eV from the energy position they have in pure Al and Al 3d-like states are totally mixed with the Co 3d states and also shift back with respect to their position in pure fcc Al. With respect to pure fcc Al, the occupied Al s-like states in the alloy are significantly modified: they are mainly present beyond 4 eV from E_F. It can also be noted that the general shape of the TB–LMTO Al 3s DOS is in better agreement with that of the LMTO calculations than that of our previous empirical TB calculations (Pécheur *et al* 1995).

Results for Al unoccupied DOS from LMTO and TB–LMTO are analogous. They show that all partial DOSs increase monotonically above E_F. Beyond E_F the unoccupied Al and Co states are completely mixed. In contrast with Co 3d states, the Co d DOS is of very faint intensity.

3. Experimental procedure and results

3.1. Principles of the techniques

Soft-x-ray emission (SXES) and soft-x-ray absorption (SXAS) spectroscopies are useful techniques for investigating DOS since they probe separately occupied and unoccupied band states (OB and UB respectively) around each constituent of a solid. Indeed, x-ray transitions involve an inner level of the solid, denoted $L_{n,l}$, and either OB or UB states. They are governed by dipole selection rules, so that s, p or d states are probed independently. Moreover, because the inner hole is on a chosen atom of the solid, the information is also site dependent. It is of interest that these techniques may be applied to any kind of solid material whatever it is: metallic, insulator, bulk, powder, thin film, ... Within the framework of the one-electron approximation, the intensities of the emitted or absorbed radiations are proportional to $|M|^2 N(\varepsilon) * L_{n,l}$ where $N(\varepsilon)$ denotes the occupied or unoccupied probed DOS. M represents the matrix element of the transition probability, it depends upon the overlap between the initial and final wave functions of the system. It is usually constant or varies slowly against energy. Thus, the shapes of the x-ray spectral distribution curves for a solid are related directly to the DOSs broadened by the Lorentzian-like energy distribution of the inner level. Therefore, no absolute DOS values are achieved from these techniques.

Each spectral distribution curve is obtained in its own x-ray transition energy scale. To gain insight into the electronic interactions in the solid it is worthwhile adjusting the SXS curves on an absolute energy scale. This may be achieved by setting E_F on each x-ray transition energy scale, which allows us to trace the various spectral distributions in the binding energy scale. It is thus necessary to know the binding energies of the various inner levels that are involved in the investigated SXES and SXAS transitions.

For such a purpose, it is very profitable to use the x-ray photoemission spectroscopy (XPS) technique. This provides the kinetic energy distribution of photoelectrons emitted from either the OB or core levels of a given sample. Calibration of the energy scale is made often by referring to the values for either the Au $4f_{7/2}$ or the contamination C 1s levels. The binding energies corresponding to OB electrons are obtained at the same time for all spectral characters and without any site selectivity. Moreover, photoemission cross sections favour d states with respect to s and p states. Accordingly, XPS cannot provide any clear view of s and p states in alloys containing simple metals and transition metals. On the contrary, it is very useful that the binding energies of the inner levels of a sample can be obtained separately because this allows to measure the binding energies of inner levels involved in the x-ray transitions which we investigate. As a consequence, the Fermi level may be placed on the various x-ray transition energy scales.

3.2. Experimental procedure

Different partial DOSs have been investigated in order to describe OB and UB states in Al_5Co_2. They are listed in table 2. Note that for Co, the Lα spectrum informs us mainly about the occupied 3d state distribution because p $\rightarrow$ d transitions are favoured with respect to p $\rightarrow$ s ones. In addition, note that the s state contribution is already significantly faint

in the OB of the pure element (Papaconstantopoulos 1986).

The SXES experiments were carried out using vacuum spectrometers fixed with bent SiO_2 $10\bar{1}0$ (Al p-like states) or RbAP (rubidium phthalic acid for Co d states) crystals or a grating (Al 3s–d states); the instrumental energy resolutions in the investigated ranges are about 0.3 eV in all cases. The final energy resolutions, as given in table 2, account for the width of the inner levels involved in the x-ray transitions. The spectra were electron stimulated from water cooled samples. The emitted photons were collected by gas flow proportional counters or both a photocathode and a channeltron. The spectral curves have been normalized between their maximum and ranges where the variation of intensity is negligible. SXES spectra of pure Al and Co were also scanned for comparison and calibration purposes.

Table 2. Analysed x-ray transition, states investigated, experimental technique, studied energy range and width of the inner level involved in the x-ray transition.

X-ray transition	Probed states	Experimental technique	Energy range (eV)	Width of inner level (eV)
Al Kα	$2p_{3/2} \rightarrow 1s$	SXES	1480–1490	
Al Kβ	OB $\rightarrow$ 1s	SXES	1545–1565	0.4
Al $L_{2/3}$	OB $\rightarrow$ $2p_{3/2}$	SXES	52–75	<0.1
Al K	1s $\rightarrow$ UB	SXAS	1555–1585	0.4
Co Lα	OB $\rightarrow$ $2p_{3/2}$	SXES	770–785	0.4

The Al K absorption edges of pure fcc Al and Al_5Co_2 were measured at the synchrotron facility of the Laboratoire pour l'Utilisation du Rayonnement Electromagnétique (LURE, Orsay, France) with the Super ACO storage ring (experimental station SA 32). The yield technique was used by means of a two-crystal monochromator equipped with SiO_2 $10\bar{1}0$ slabs. The instrumental energy resolution was also about 0.3 eV. These Al K spectra were normalized in the intensity scale as will be mentioned in the next paragraph.

We measured directly the Al $2p_{3/2}$ and Co $2p_{3/2}$ binding energies but could not obtain that of the Al 1s because the energy of the incident radiation in the XPS spectrometer was not high enough. Thus, the Al 1s binding energy was deduced from the energies of both the Al $2p_{3/2}$ and the Al Kα ($2p_{3/2} \rightarrow 1s$) x-ray emission line (Traverse *et al* 1988).

3.3. Results

According to our experimental accuracy, we found that the binding energy of the Co $2p_{3/2}$ inner level for the alloy is the same as in pure Co whereas the Al inner levels are shifted by 0.3 eV in Al_5Co_2 with respect to pure fcc Al. Thus, finally, we could place E_F on the various x-ray transition energy scales within ± 0.3 eV for Co and ± 0.2 eV for Al. The curves corresponding to the Co 3d, Al 3p, Al 3s–d and Al p spectral distributions adjusted in the binding energy scale are shown in figures 2 and 3.

The Co 3d curve retains an almost symmetric shape, as in the pure metal. With comparison to pure Co, the maximum intensity is at 1.7 ± 0.1 eV from E_F, i.e. shifted by about 0.2 eV towards increasing x-ray transition energies. The full width at half maximum intensity (FWHM) is 2.8 ± 0.1 eV in the alloy, i.e. reduced by about 0.5 eV with respect to the pure metal (figure 3).

OB states extend over about 12 eV. Whereas the intensity of the Al 3p states distribution curve decreases rapidly beyond 4 eV from E_F, that of the Al 3s–d distribution remains

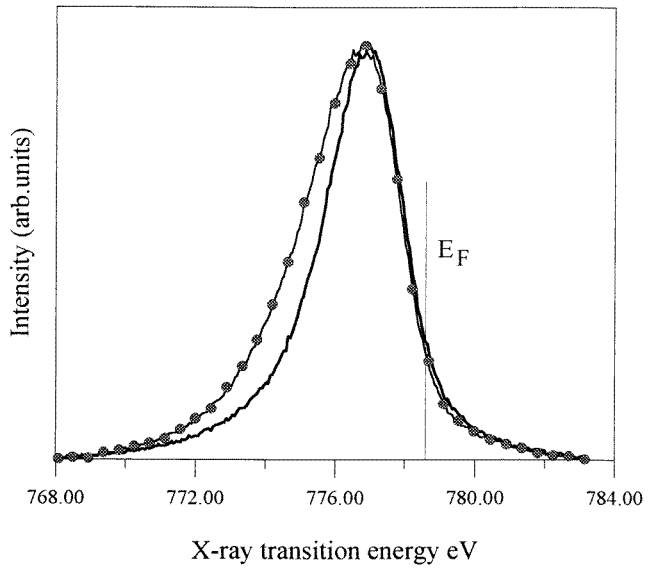

Figure 2. Occupied Co 3d distribution curves in pure cobalt (dotted line) and in Al_5Co_2 (full line).

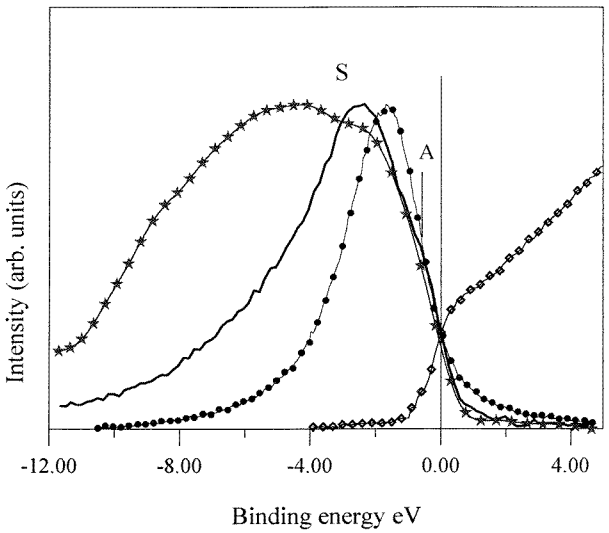

Figure 3. Al and Co occupied and Al unoccupied electronic distribution curves in Al_5Co_2: full line, Al 3p; stars, Al 3s–d; dots, Co 3d; squares, Al p.

significant over almost the whole energy range. This gives an indication that the states are somewhat hybridized near E_F whereas states far below are almost pure s-like in character. The maximum of the Al 3p sub-band is at 2.5 ± 0.1 eV from E_F. Within the experimental accuracy, the Al 3p and Al 3s–d curves edges close to E_F overlap over all their extent that

covers about 1 eV from E_F. They display a change of slope at 0.7 ± 0.1 eV from E_F, labelled A on the figure. The intensity of the Al 3s–d distribution slightly increases after feature S, which corresponds to the energy where the intensity of the Al 3p distribution decays. Its maximum is at about 5.3 eV below E_F. The Co 3d distribution overlaps the Al sub-band edges, thus emphasizing the Al and Co interaction in the vicinity of E_F.

The Al p distribution curve is also plotted in this figure. Its intensity, which is adjusted to the value of the Al 3p distribution at E_F, increases monotonically beyond the absorption jump.

4. Discussion

Let us recall that the curves are normalized to unity at their maximum intensity. For pure fcc Al, the inflexion point of the steep Al 3p edge is exactly at E_F and its intensity is 0.5. In Al_5Co_2, the Al 3p edge is less steep than in the pure metal. The point corresponding to half the maximum intensity is at 0.45 ± 0.05 eV from E_F. The intensity of the Al 3p sub-band at E_F is 0.3 against 0.5 in pure fcc Al. All this indicates the formation of a pseudogap at E_F in the Al states distribution. Let us recall that we have observed a larger and wide pseudogap in related decagonal phases: indeed, the intensities at E_F and the distances to E_F of the point corresponding to half the maximum intensity are 0.2 and 0.55 eV in $Al_{65}Cu_{15}Co_{20}$ and 0.17 and 0.60 eV in $Al_{70}Cu_{15}Co_{15}$ (Belin-Ferré *et al* 1996). This is consistent with previous observations that the pseudogap is more marked in icosahedral quasicrystals than in approximants, although the difference may be rather small (Belin *et al* 1994, Belin-Ferré *et al* 1997).

For meaningful comparison between experimental data and theory, we have calculated x-ray spectra (denoted by CS in the following) by calculating in each case the convolution product of the calculated partial DOSs by the Lorentzian-like energy distribution of the inner level that participates in the x-ray transition and then by a Gaussian distribution to account for the instrumental function of the various spectrometers. The FWHMs of the Lorentzian functions were taken equal to 0.4, 0.1 and 0.4 eV respectively for Al 3p, Al 3s and 3d and Co 3d levels according to Krause and Oliver (1979). The FWHM of the Gaussian distribution was taken in all cases as equal to 0.3 eV. The calculated x-ray curves are plotted in figure 4(a) and (b) for LMTO and TB–LMTO calculations respectively. Each curve is normalized to its own maximum intensity. For the sake of comparison, the corresponding experimental curves are displayed on the same figure; they are normalized to the maximum intensity as well. For the Al 3s–d spectra, a better adjustment of calculations to the experimental results requires us to consider the differences in $p \rightarrow s$ and $p \rightarrow d$ transition probabilities. This may be achieved in principle by adding only one fraction of the total calculated d contribution, namely two-fifths, to the s one before performing the different convolutions (Goodings and Harris 1969). We did so but could not obtain a satisfactory agreement between CS and experiment. This is shown in figure 4(a). We will not discuss this point here; it is still a matter of investigation by theoreticians (Papaconstantopoulos 1997).

Each figure contains the three panels: from bottom to top, these display Al 3p and Al p curves, then Al 3s–d and finally Co 3d curves respectively. Figure 4(a) corresponds to the LMTO calculation. The LMTO CSs are in rather good agreement with experiment. The shapes of the Co 3d curves are similar, the two maxima coincide and the FWHMs differ only by about 0.3 eV. This may be explained by the fact that satellite emissions from multi-ionized atoms may contribute to the experimental curve towards increasing x-ray transition energies. The CS Al 3p and Al 3d curves fit rather well the low-energy part of the edge

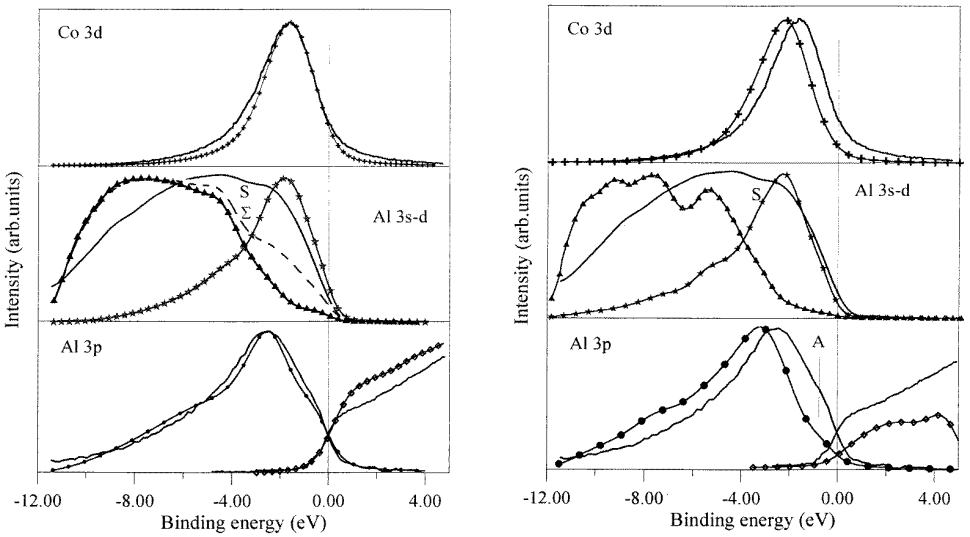

Figure 4. (a) A comparison between calculated curves from LMTO DOSs (see the text) and the experimental electronic distribution: top panel, Co 3d states (full line, experimental; crosses, calculated); middle panel, Al 3s–d states (full line, experimental; triangles, calculated Al 3s; stars, calculated Al 3d; dashes, calculated $s + \frac{2}{5}d$—see text; bottom panel, Al 3p states (left-hand side full line, experimental; dots, calculated) and Al p states (right-hand side full line, experimental; diamonds, calculated). (b) A comparison between calculated curves from combined TB–LMTO DOSs (see the text) and experimental electronic distributions: top panel, Co 3d states (full line, experimental; crosses, calculated); middle panel, Al 3s–d states (full line, experimental; triangles, calculated Al 3s; stars, calculated Al 3d); bottom panel, Al 3p states (left-hand side full line, experimental; dots, calculated) and Al p states (right-hand side full line, experimental; diamonds, calculated).

of the experimental curves and consequently account for the intensities at E_F; the maxima of the CS and experimental Al 3p curves coincide although the CS curve is sharper than in experimental. The Al p CS and experimental curves display a $\tan^{-1}$-like absorption jump and similar shape above E_F. Beyond 1 eV from E_F, adjusting the intensities of the absorption curves to the values of the occupied counterparts at E_F, the experimental curve is below the CS but increases in the same way versus energy. There is not such a good agreement between the experimental Al 3s–d curve and the CS Al 3s one beyond -6 eV from E_F. However, the faint hollow S of the experimental Al s–d curve coincides with the feature marked Σ of the curve calculated according to Goodings and Harris (1969), i.e. with the energy of the crossing between the partial Al s and Al d CS curves.

Let us now pay attention to the TB–LMTO. Whereas the shapes and FWHMs of the CS and experimental Co 3d curves are the same, the respective maxima are shifted by about 0.6 eV. Moreover, the maxima of the CS and experimental Al 3p curves are shifted by about 0.8 eV. These shifts are related to the broader range within which the DOS is minimum near E_F in the TB–LMTO calculation when compared with the LMTO calculation (figures 1(a) and 1(b)). Note also that the shapes of the edges near E_F of the latter curves differ since the CS one displays a wide faint hollow almost at the energy of the change of slope A of the experimental curve which is not accounted for.

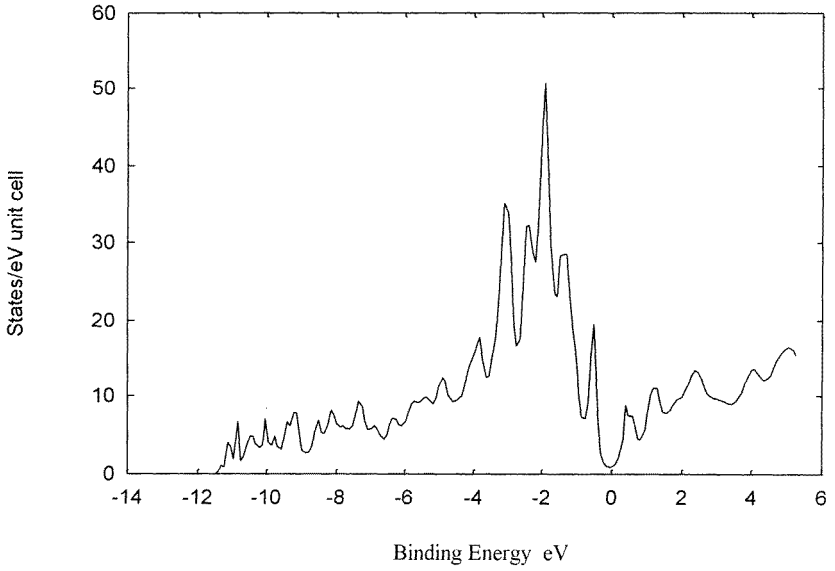

(a)

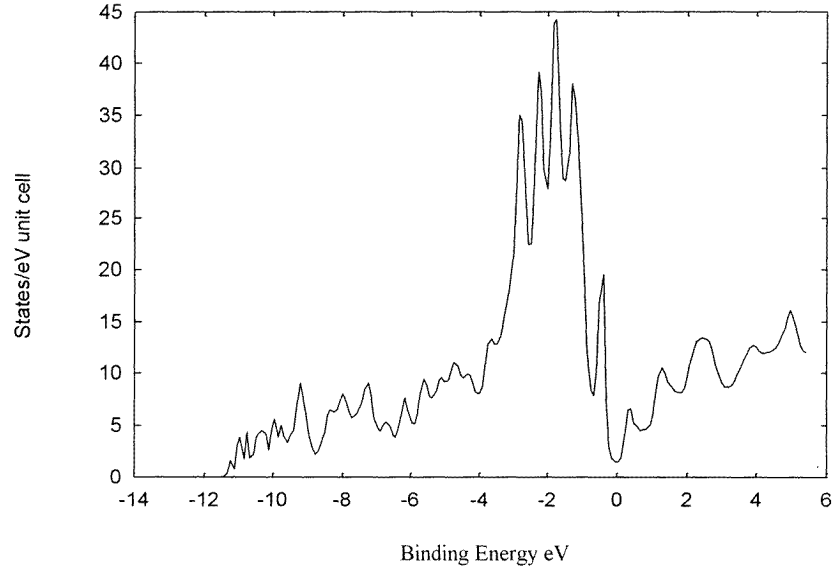

(b)

Figure 5. (a) Total TB–LMTO DOS using the full self-consistent potential parameters of the LMTO–ASA calculation, instead of the tabulated ones. (b) Total TB–LMTO DOS using a modified interpolation formula for the structure constants (see the text).

To investigate the possible origin of these discrepancies between LMTO and TB–LMTO calculations, we have performed two further TB–LMTO calculations (figure 5). First, we have used the self-consistent potential parameters of the full LMTO calculation, instead of those deduced from Andersen tables. The corresponding total DOS is shown in figure 5(a), and it is rather similar to the one of figure 1(b). This shows that self-consistency is not

the main origin of the discrepancies (the sets of potential parameters differ by less than 12%). Then, since the potential parameters seemed satisfactory, we have investigated the structure constants. The calculation of figure 1(b) relies on the two-centre interpolation formula given by Andersen *et al* (1987) to obtain the TB non-diagonal structure constants in real space as functions of the reduced distance d/w between atoms (d is the distance and w the mean atomic radius in the structure). This interpolation formula compared well with the exact results for the first neighbours in the FCC and BCC structures ($d/w = 1.809$ and 1.759), but it overestimates somewhat the sdσ, pdσ and ddσ values for the first neighbours in the simple cubic structure ($d/w = 1.612$). In the Al_5Co_2 structure, each atom has three to nine close neighbours with a $d/w < 1.759$, so that the interpolation formula may lead to an overestimate of s–d, p–d and d–d hybridizations. To verify this, we have performed a TB–LMTO calculation with another interpolation formula with a different functional form (that is $A(d/w)^{\alpha}\exp(-\beta d/w)$ instead of $A\exp(-\beta d/w)$). This formula reproduces well the FCC and BCC σ structure constants and leads to values only slightly lower than the exact ones for the simple cubic structure. The results for the total DOS are shown in figure 5(b). As foreseen, the hybridizations are decreased and the width of the quasi-gap and of the d-like region of the DOS are reduced. This decreases the shifts of the CS of figure 4(b) with respect to the experimental curves, improving their agreement.

5. Conclusion

Combining SXS and XPS techniques we have investigated Al and Co electronic distributions in Al_5Co_2. We have shown that Al–Co interaction takes place near E_F, the result of which is to repel the Al 3p states from E_F by about 1 eV. Thus a pseudo-gap is formed at E_F. The states within 5 eV from E_F are in interaction with Co states and beyond 5 eV, they are almost Al s pure in character. The comparison between the experimental results and calculations has pointed out a rather good agreement with LMTO calculations. Such an agreement with LMTO results is in line with the fact that this is a more elaborate band structure calculation.

The agreement is only acceptable with TB–LMTO, but the main differences between TB–LMTO and LMTO (the shifts in the CS of figure 4(b)) appear to be due to the interpolation formula used for the structure constants. This can be corrected and TB–LMTO calculations should be useful in those cases, listed in the introduction, where full LMTO calculations cannot be performed as easily.

Acknowledgments

Support from the Institut National Polytechnique de Lorraine and by the Austrian Ministry of Research East–West Co-operation Contract under the title ‘Soft-x-ray emission spectroscopy of metallic systems’ is warmly acknowledged. We are grateful to Professor H Kirchmayr and Doctor H Müller for their hospitality at the Technical University in Vienna. We are indebted to D Nguyen Manh and D Mayou for help during the LMTO calculation and to G Toussaint for his participation in the TB calculation. We thank Z Dankhazi for assistance during experiments.

References

Andersen O K 1975 *Phys. Rev.* B **12** 3060

Andersen O K, Jepsen O and Glötzel D 1985 *Highlights of Condensed Matter Theory* ed F Basani, F Fumi and M Tosi (New York: North-Holland)

Andersen O K, Jepsen O and Sob M 1987 *Electronic Band Structure and its Applications* ed M Yussouff (Berlin: Springer) p 1

Belin E, Dankázi Z, Sadoc A, Dubois J M and Calvayrac Y 1994 *Europhys. Lett.* **26** 677

Belin-Ferré E, Dankázi Z, Fournée V, Sadoc A, Berger C, Müller H and Kirchmayr H 1996 *J. Phys.: Condens. Matter* **8** 6213

Belin-Ferré *et al* 1997 *Proc. 6th Int. Conf. on Quasicrystals* ed T Fujiwara (Singapore: World Scientific) at press

Berger C 1994 *Lectures on Quasicrystals* ed F Hippert and D Gratias (Les Ulis: Les Editions de Physique) pp 463–504 and references therein

Goodings D A and Harris R 1969 *J. Phys. C: Solid State Phys.* **2** 1808

Haydock R 1980 *Solid State Physics* vol 35 ed H Ehrenreich, F Seitz and D Turnbull (New York: Academic) p 87

Hedin L and Lundqvist B I 1971 *J. Phys. C: Solid State Phys.* **4** 2064

Jepson O and Andersen O K 1971 *Solid State Commun.* **9** 1763

Krause M O and Oliver J H 1979 *J. Phys. Chem. Data* **8** 329

Newkirk J B, Black P J and Damjanovic A 1961 *Acta Crystallogr.* **14** 532

Papaconstantopoulos D A 1986 *Handbook of the Band Structure of Elemental Solids* (New York: Plenum) p 208 for Al and p 109 for Co.

Papaconstantopoulos D A 1997 private communication

Pécheur P, Belin E, Toussaint, Trambly de Laissardière G, Mayou D, Dankházi Z, Müller H and Kirchmayr H 1995 *Proc. 5th Int. Conf. on Quasicrystals* ed C Janot and R Mosseri (Singapore: World Scientific) p 501

Quivy A, Quiquandon M, Calvayrac Y, Faudot F, Gratias D, Berger C, Brand R A, Simonet V and Hippert F 1996 *J. Phys.: Condens. Matter* **8** 4223

Song S and Ryba E R 1992 *Phil. Mag. Lett.* **65** 85

Terakura K 1977 *J. Phys. F: Met. Phys.* **9** 1773

Trambly de Laissardière G, Nguyen Mahn D, Magaud L, Julien J P, Cyrot-Lackmann F and Mayou D 1995 *Phys. Rev.* B **52** 7920

Traverse A, Dumoulin L, Belin E and Sénémaud C 1988 *Quasicrystalline Materials* ed C Janot and J M Dubois (Singapore: World Scientific) p 399